J Mater Sci: Mater Med (2010) 21:463–472
DOI 10.1007/s10856-009-3919-6

Modelling Young's modulus for porous bones with microstructural variation and anisotropy

Jianfeng F. Wang

Received: 16 May 2009 / Accepted: 19 October 2009 / Published online: 1 November 2009

Abstract A structural model with three compositional phases and two levels of hierarchical organization is proposed for predicting Young's modulus of porous bones with microstructural variations and anisotropy based on their geometric similarity to metal foams. It has been shown that the proposed single model provides predictions of Young's modulus with high accuracy up to ±30% for cortical and cancellous bones compared with measured data from the literature. In addition, the conversion of the solid bone shape from "Plate-like" to "Rod-like" at a porosity of 70% or higher (*BV/TV* 30% or lower)—verified by observations—can be predicted using the proposed model.

1 Introduction

Bone is a heterogeneous and anisotropic material featuring a multilevel hierarchical structure. Its fundamental function is clearly mechanical. At the macroscopic level, bones can have different structures depending on their respective functions such as protecting internal organs, supporting the body, working together with other components to generate and transfer forces for movement, and helping sound transduction for hearing [1]. Some bones are very dense and some are very spongy. The pores of those bones are generally composed of blood, fat, water and/or some gases. The concept of "porous bone" in this paper is intended to be general and encompass all sorts of cortical and cancellous bones consisting of identifiable pores and solid materials. At the lower level of the hierarchy, the solid bone material is a composite of organic phase including triple helix type I collagen with some lipids and water and a dispersed inorganic phase of staggered parallel platelet mineral particles. An understanding of the geometric structures and mechanical properties of bones is important for diagnosis of diseases and other problems affecting bones such as osteoporosis [1]. Young's modulus of elasticity is a fundamental mechanical property of bone in terms of its stiffness. Physically, Young's modulus of a typical heterogeneous material like bone depends on its component compositions and microstructure [2]. The prediction of Young's modulus and other mechanical properties is of great significance due to the complexity and high cost of accurate measurements.

For modelling Young's modulus or other properties, some fundamental structural models are often preferable due to the ease of calculations and reliability of their physical basis [2]. However, none of the fundamental structural models, including the Parallel, Series, two forms of Maxwell–Eucken (ME) [3], Effective Media Theory (EMT) [4], or the recently proposed Co-Continuous (CC) model [5], were able to accurately predict the apparent properties of porous materials over the full range of porosities [6, 7]. For porous bones, power-law equations are widely used to fit measured data [8]. For other porous materials, such as metal foams, a similar method is to use empirical models which are generally obtained by modifying these fundamental structural models by including what is essentially a fitting parameter [9]. However, those empirical models usually have limited applicability [7, 10]. An alternative is to perform rigorous numerical simulations using finite difference or finite element methods such as [11, 12] in order to describe the geometry of the structure accurately; however, such models place heavy demands on time and resources. Often the most attractive option is to use simple algebraic models with a well-established physical

J. F. Wang (✉)
School of Engineering and Advanced Technology, Massey University, Private Bag 11-222, Palmerston North, New Zealand
e-mail: J.F.Wang@massey.ac.nz

basis due to their simplicity, low cost, and reasonable accuracy, even when the microstructure is not known with certainty [6, 7].

Moreover, one structural model generally applies for only one specific structure. For many synthetic and natural materials such as bones, however, the microstructure varies considerably even at a specific porosity for the same sorts of materials [8]. Therefore, it is important to quantify the effect of the structural variations on the properties of the specific bone. Figure 1a–c show the three common structures of porous bones which are characterised by different solid bone shapes, that are "plate-like", "rod-like", or a combination of these. Many observations such as [13–19] have confirmed that the overall morphology of porous bones is more "plate-like" at low porosities and more "rod-like" at high porosities, and the microstructure alteration from "plate-like" to "rod-like" is likely to be due to aging or disease [19, 20].

Furthermore, the structural variations and high structural anisotropy of porous bones at several length scales lead to the extreme mechanical anisotropy. The value difference of Young's modulus between different orientations is as large as 10–20 folds [21]. In this paper, the focus is on modelling Young's modulus for porous bones with microstructure variations and anisotropy.

2 Materials and methods

2.1 Structural model

The following three-phase and two-level structure is proposed for simplifying the hierarchical organization of all sorts of porous bones:

(1) A porous bone is composed of solid bone materials (solid phase) and pores (fluid phase);
(2) The solid phase is composed of an organic matrix phase (collagen with lipids and water) and an inorganic dispersed phase (mineral particles).

For the first level of structure, most porous bones have plate-like, rod-like or combined structures, depending on their porosities, as assessed in many observations [13–20]. To determine the two boundaries of such mixed structures, one is related to the rod-like solid bone structure. By comparing Fig. 1a with d, one can see that the rod-like structure is very similar to the open cell metal foam. Moreover, the open cell metal foam structure can be modelled with reasonable accuracy by a Symmetric and Interconnected Skeleton Structure (SISS) as shown in Fig. 1g according to the recent work by the author and his coworkers [7]. The SISS is an ideal open cell structure with a maximum scale of connectivity and symmetry between the pores and solid phase [7]. Therefore, the SISS can be regarded as a boundary structure of porous bones with maximum connectivity and symmetry between the solid bones and the pores.

The other boundary structure is related to the plate-like solid bone structure as shown in Fig. 1c, which is very similar to the closed cell metal foams as shown in Fig. 1f [22]. It can be seen from Fig. 1c and f that interconnected ellipsoidal pores exist between the plate-like solid bones. Moreover, the structure can be simplified to have point-contact ellipsoidal pores, that is the basic structure of the three-point (3P) model [2], as shown in Fig. 1h. Even though real trabecular bones never have absolutely closed pores, the connectivity between their pores varies considerably, being likely to be very low—for instance—for some cortical bones. Therefore, it appears to be reasonable that the point-contact pore structure represents a boundary structure of porous bones with a minimum scale of connectivity and symmetry between the pores and solid bones.

In addition, the plate-like and rod-like combined structure of porous bones is also similar to the semiopen cell metal foams [23] as shown in Fig. 1b and e, respectively. Therefore, the varied structure of porous bones can be assumed to be a composite structure with different fractions of SISS and 3P model structures based on the structural similarity between porous bones and metal foams. This conjecture implies that the apparent Young's modulus of a porous bone (E_a) is bounded by the two model values at a specific direction:

$$E_a = (E_{SISS},\ E_{3P}) \tag{1}$$

To quantify the mechanical anisotropy, the structural anisotropy needs to be defined. As shown in Fig. 1g and h, the average side length ratios for the units at z and y directions are defined by:

$$l_z = \sum_{i=1}^{N} \frac{c_i}{a_i}/N \tag{2}$$

$$l_y = \sum_{i=1}^{N} \frac{b_i}{a_i}/N \tag{3}$$

while a, b, c and N stand for the unit sizes at x, y and z directions respectively and the number of the unit.

The structural anisotropy scale at z and y directions relative to that at x direction is defined by:

$$\delta_z = (l_z - 1) \cdot 100\% \tag{4}$$

$$\delta_y = (l_y - 1) \cdot 100\% \tag{5}$$

while x direction is taken as a reference so $l_x = 1.0$ and $\delta_x = 0$.

For a three dimensional isotropic materials, $\delta_x = \delta_y = \delta_z = 0$.

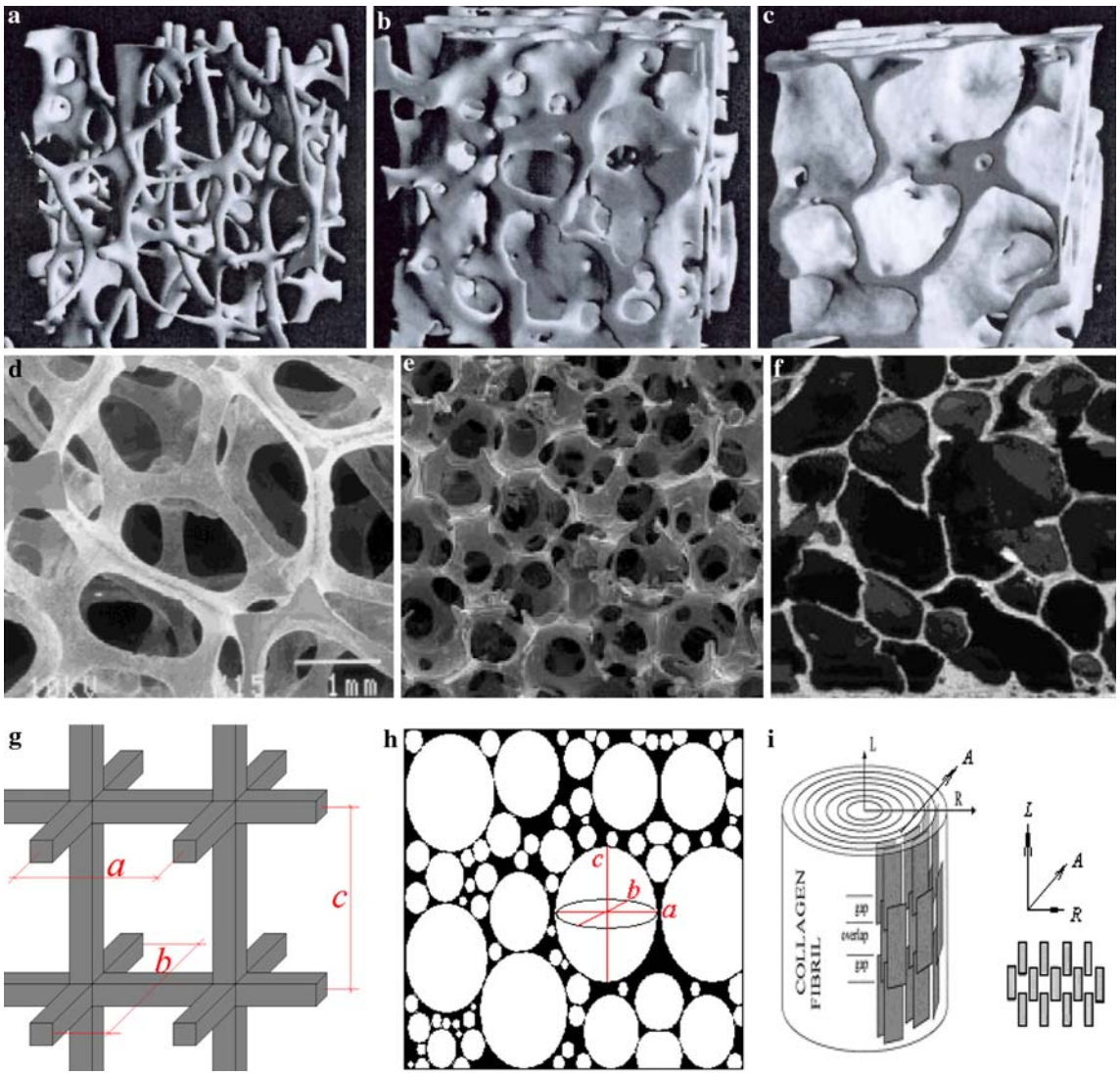

Fig. 1 Bones **a** with interconnected rod-like solid bones ($BV/TV = 8.5\%$), **b** with interconnected rod-like and plate-like combined solid bones ($BV/TV = 12\%$), and **c** with plate-like solid bones and approximately ellipsoidal pores ($BV/TV = 26\%$) [13]. Aluminium foams **d** with open cells (porosity $P = 92\%$, Duocel Al foam), **e** with semiopen cells ($P = 90\%$) [23] and **f** with closed cells ($P = 75\%$) [22]. Model structures **g** with symmetric and interconnected skeleton structure (SISS) [7] for open cell foams, and **h** with point-contact ellipsoidal pores (i.e. 3P structure [2]) for closed cell foams. Solid bone structure model **i** with platelet minerals aligned in collagen matrix [25]

The isotropic SISS model has been described in detail in [7]. With a similar method, the isotropic SISS model can be extended to an anisotropic model. As the void phase has a Young's modulus far less than that of the solid bone phase, the corresponding anisotropic SISS model equations at z, y, and x directions are:

$$\frac{E_{SISS-z}}{E_{B-z}} = \frac{e^2}{(1+\delta_y)} \tag{6}$$

$$\frac{E_{SISS-y}}{E_{B-y}} = \frac{e^2}{(1+\delta_z)} \tag{7}$$

$$\frac{E_{SISS-x}}{E_{B-x}} = \frac{e^2}{(1+\delta_y)(1+\delta_z)} \tag{8}$$

where $E_{SISS\text{-}x}$, $E_{SISS\text{-}y}$, and $E_{SISS\text{-}z}$ stand for the apparent Young's modulus of porous bones, $E_{B\text{-}x}$, $E_{B\text{-}y}$, and $E_{B\text{-}z}$ stand for the Young's modulus of solid bones at x, y, and z directions respectively, and e stands for the average side length of solid bones cross-section and can be obtained from the following equation:

$$(3+\delta_y+\delta_z)e^2 - 2e^3 = (1+\delta_y)(1+\delta_z)BV/TV \tag{9}$$

For isotropic structure of SISS model, the equation at x, y, or z direction is [7]:

$$\frac{E_{SISS}}{E_B} = \left(0.5 - \cos\left(\frac{\pi + \arccos(1-2BV/TV)}{3}\right)\right)^2 \tag{10}$$

where *BV/TV* is the volume fraction of solid bone strut within the porous bone.

Similarly, due to the Young's modulus of pores (fluid phase) far less than that of solid bones, the equation of the 3P model with ellipsoidal pores [2] is:

$$\frac{E_{3P}}{E_B} = \frac{(d-1)(BV/TV)^2}{1+(d-2)BV/TV} \tag{11}$$

where the dimension number d at a specific direction can be accurately determined with the length ratios of three axles of an ellipsoid [24]. For probate pores, specifically, $\delta_x = \delta_y = 0$ and $\delta_z > 0$, the dimension number at x or y direction can be approximated by [24]:

$$d_x = d_y = \frac{2}{(1-p^{-2})^{-1} - 0.5p^{-2}(1-p^{-2})^{-1.5} LN\left(\frac{1+(1-p^{-2})^{0.5}}{1-(1-p^{-2})^{0.5}}\right)} \quad (p = 1+\delta_z) \tag{12}$$

For oblate pores, $\delta_x = \delta_y = 0$ and $\delta_z < 0$, the dimension number at x or y direction is approximated by [24]:

$$d_x = d_y = \frac{2(1-p^2)^{1.5}}{p\cos^{-1}(p) - p^2(1-p^2)^{0.5}} \quad (p = 1+\delta_z) \tag{13}$$

For any three-dimensional structure, the dimension number at x, y and z directions has the relation:

$$d_x^{-1} + d_y^{-1} + d_z^{-1} = 1 \tag{14}$$

For any isotropic material, $\delta_x = \delta_y = \delta_z = 0$, the dimension number has the relation:

$$d_x = d_y = d_z = 3 \tag{15}$$

The apparent density of porous bone (ρ_a) has the following relation:

$$\rho_a = \rho_B BV/TV + \rho_v P \tag{16}$$

The volume fractions of the solid phase (*BV/TV*) and pores (the porosity P) have the relation:

$$BV/TV + P = 1 \tag{17}$$

For the second level of structure, the solid bone is composed of an organic phase of collagen (as well as water and lipids for fresh bones) and an inorganic phase of staggered parallel platelet mineral particles, as shown in Fig. 1i [25]. The revised model based on the ME model applies for Young's modulus [6]:

$$E_B = \frac{E_{apa}v_{apa}\frac{dE_{org}}{(d-1)E_{org}+E_{apa}} + E_{org}v_{org}}{v_{apa}\frac{dE_{org}}{(d-1)E_{org}+E_{apa}} + v_{org}} \tag{18}$$

where E_{apa}, v_{apa} and E_{org}, v_{org} stand for the Young's modulus and volume fractions of apatite and organic phase respectively, and the dimension number d is determined by the plate aspect ratio (*AR*) [24]. When $AR \gg 1$, the longitude (L) and azimuth (A) direction dimensions are:

$$d_l = \frac{AR_l \cdot AR_a + AR_l + AR_a}{AR_a} \tag{19}$$

$$d_a = \frac{AR_l \cdot AR_a + AR_l + AR_a}{AR_l} \tag{20}$$

The corresponding dimension number at the radial (R) direction can be obtained by:

$$d_r = \left(1 - d_l^{-1} - d_a^{-1}\right)^{-1} \tag{21}$$

Bone solid phase is essentially anisotropic as shown in Fig. 1i [25]. The calculations of Young's modulus for the anisotropy at the second level of structure can be conducted using the different dimension numbers at longitude, azimuth and radial directions separately.

Solid bone has the following density relation:

$$\rho_B = \rho_{apa}v_{apa} + \rho_{org}v_{org} \tag{22}$$

The volume fractions of the collagen and the apatite particle have the relation:

$$v_{apa} + v_{org} = 1 \tag{23}$$

The mineral (ash) ratio (*MR*, mass fraction of mineral to the whole porous bone, g/g) or calcium ratio (*CR*, mass fraction of calcium to the whole porous bone, g/g), and the apparent mineral (ash) density (*MD*, g/cm^3) or apparent calcium density (*CD*, g/cm^3), are often measured for obtaining the composition of bones. The volume fraction of mineral particles is obtained by:

$$v_{apa} = \frac{MR/\rho_{apa}}{MR/\rho_{apa} + (1-MR)/\rho_{org}} \tag{24}$$

In addition, calcium has a mass fraction of about 40% in the three sorts of apatite (39.8% for hydroxyapatite, 39.7% for fluorapatite and 38.5% for chlorapatite), so the mineral ratio *MR* can be obtained from the measured calcium content *CC*:

$$MR = CR/0.4 \tag{25}$$

MD and *CD* have the following relations:

$$MD = MR \cdot \rho_a \tag{26}$$

$$CD = CR \cdot \rho_a \tag{27}$$

With the proposed three-phase and two-level structure for a porous bone, the two bounds on the Young's modulus can be determined specifically if the structural anisotropy and any two of the following four composition parameters of components are measured or provided in advance:

(a) apparent density (ρ_a), (b) mineral ratio (*MR*) or calcium ratio (*CR*), (c) mineral density (*MD*) or calcium density (*CD*), and (d) porosity (*P*) or solid bone volume fraction (*BV/TV*).

2.2 Component properties and geometric parameters

For the modelling calculations, the following component properties and structural parameters were selected:

(1) *Density*: Pure mineral/apatite $\rho_{apa} = 3.15$ g/cm^3 and organic phase $\rho_{org} = 1.41$ g/cm^3 from the literature [26, 27]. The pores $\rho_v = 0$ g/cm^3.

(2) *Young's modulus*: Pure mineral/apatite $E_{apa} = 125$ GPa, organic phase $E_{org} = 1$ GPa, and pores $E_v = 0$ GPa. The measured Young's modulus for the three sorts of apatite ranges from 100 to 150 GPa according to the literature [28–33], so an average value was used in this work. The measured value of collagen fibrils differs in magnitude up to four orders from 1 MPa to 25 GPa depending on the test methods, test conditions (air temperature and humidity) and the sample states (hydrated or dehydrated) [27, 34–36]. $E_{org} = 1$ GPa corresponds to an average value of organic phase in bones at a room air condition. For the pores, generally composed of air for dry bones and some amount of liquids for fresh bones, Young's modulus is far less than it is for solid bone, so $E_v = 0$ GPa appears to be a reasonable choice.

(3) The aspect ratios of platelet mineral particles: $AR_l = 30$ and $AR_a = 15$. As reviewed [2] and observed [37] recently, $AR_l = 30$ and $AR_a = 15$ look to be good estimates for the average values of respect ratios for mineral particles aligned in collagen fibrils. The anisotropy of solid bones at the second level of structure can be determined using these aspect ratios [24].

(4) The anisotropic scale at the first level of structure is not available for most porous bones from the literature. In this work, the predictions were conducted using positive structural anisotropy at a unique direction z while isotropic structures were assumed for the other two directions x and y, that is $\delta_x = \delta_y = 0$, and $\delta_z > 0$. This assumption appears to be reasonable because most bones are mechanically loaded at a unique direction, such as the primary axial direction.

2.3 Data sources

A large number of measured data on the Young's modulus of porous bones are available from the literature. However, most publications present only one parameter, such as apparent density in [38, 39]. As mentioned in Sect. 2.1, at least two parameters for component compositions except the anisotropy at the first level of structure are required for defining the modulus of a specific porous bone using the proposed three-phase and two-level structural model. In this work, 90 data from porous bones of 20 species, including both humans and animals, were collected from 8 publications [40–47]. Of the 90 data collected, 70 proximal or distal-measured Young's modulus ranges from 5 to 35 GPa with porosities from 3 to 40%, and 20 medial or lateral-measured Young's modulus ranges from 0.15 to 0.45 GPa with porosities from 40 to 80%.

Moreover, though only apparent density data were provided in some data sources [38, 44], the common range of a component parameter known for general bones, allows us to predict the range of Young's modulus using the proposed model.

In addition, there is no detail information available from the 8 sources [40–47] about the anisotropy of the measured bones at the first level of structure.

2.4 Modelling calculations

On the modelling calculations with two component parameters provided, the first step is to determine the three dimensional anisotropy at the first level of structure using Eqs. 2–5. For predicting the Young's modulus at proximal/distal direction:

(1) Use Eqs. 22–27 to calculate the volume fractions of apatite and organic phase, and then use Eq. 19 to calculate dimension number d_l and use Eq. 18 to calculate the solid bone Young's modulus at the second level of structure $E_{B\text{-}l}$;

(2) Use Eqs. 12 and 14 to calculate d_z, and then use $E_{B\text{-}l}$ to replace $E_{B\text{-}z}$ in Eq. 11 to calculate $E_{3P\text{-}z}$;

(3) Use Eq. 9 to calculate e and then use $E_{B\text{-}l}$ to replace $E_{B\text{-}z}$ in Eq. 6 to calculate $E_{SISS\text{-}z}$.

Similarly, for predicting the Young's modulus at lateral/medial direction:

(1) Use Eqs. 22–27 first to calculate the volume fractions of apatite and organic phase, and then use Eqs. 19–21 to calculate dimension number d_r and use Eq. 18 to calculate the solid bone Young's modulus at the second level of structure $E_{B\text{-}r}$;

(2) Use Eq. 12 to calculate d_x, and then use $E_{B\text{-}r}$ to replace $E_{B\text{-}x}$ in Eq. 11 to calculate $E_{3P\text{-}x}$;

(3) Use Eq. 9 to calculate e and then use $E_{B\text{-}r}$ to replace $E_{B\text{-}x}$ in Eq. 8 to calculate $E_{SISS\text{-}x}$.

3 Results

The proposed model incorporates two submodels, SISS and 3P at the first level of structure and one submodel at the

second level of structure. The three-dimensional anisotropy of porous bones at two levels of structure has been included in the modelling calculations using submodel equations.

3.1 Effect of structural variations and anisotropy

Figure 2a and b show the effect of structural variations between the SISS and 3P for isotropic structures at the first level of structure ($\delta_x = \delta_y = \delta_z = 0$). In order to understand the effect of anisotropy at a unique direction, Fig. 3a–d show the comparison between the SISS and 3P models for the anisotropy at z direction δ_z ranging from 0 to 70% and isotropic structures assumed at x and y directions ($\delta_x = \delta_y = 0$) at the first level of structure.

From Figs. 2a, b and 3a–d, one can see that the SISS model value is greater than the 3P model value when the porosity is greater than 70%, and the SISS model value is less than the 3P model value when the porosity is less than 70%. At a porosity of 30% ($BV/TV = 70\%$), the difference between the SISS model and the 3P model values attains maximal value for porosity of less than 70% ($BV/TV > 30\%$). When porosity is greater than 70% ($BV/TV < 30\%$), the difference between the two models becomes increasingly greater with an increase in porosity, as can be seen much clearly in Fig. 2b expressed in a logarithmic coordinate. This means that the effect of the solid bone shape on the stiffness of bones is much more pronounced at a higher porosity (>70%) than at an intermediate or lower porosity (<70%).

As shown in Fig. 3a and b, with the increase in anisotropic scale in the loading direction z, the 3P-SISS bounds become narrower at z direction and wider at x or y direction when BV/TV is greater than 30%; but when BV/TV is less than 30%, the 3P-SISS bounds become wider at z direction and narrower at x or y direction. Figure 3c and d show the ratios of anisotropic to isotropic model values for different anisotropy at the first level of structure.

3.2 Predictions compared with measured data

Figure 4a shows the measured data from the literature compared with the predictions made using anisotropic model at the second level of structure, and using isotropic SISS and 3P models at the first level of structure. Figure 4b shows the predictions made using anisotropic models at both levels of structure ($\delta_z = 50\%$). From Fig. 4a and b, it is found that the prediction accuracy has been improved from ±50 to ±30% by including the anisotropy ($\delta_z = 50\%$) at the first level of structure in the modelling.

For porous bones with only one component parameter known, the proposed model can be used for predicting the

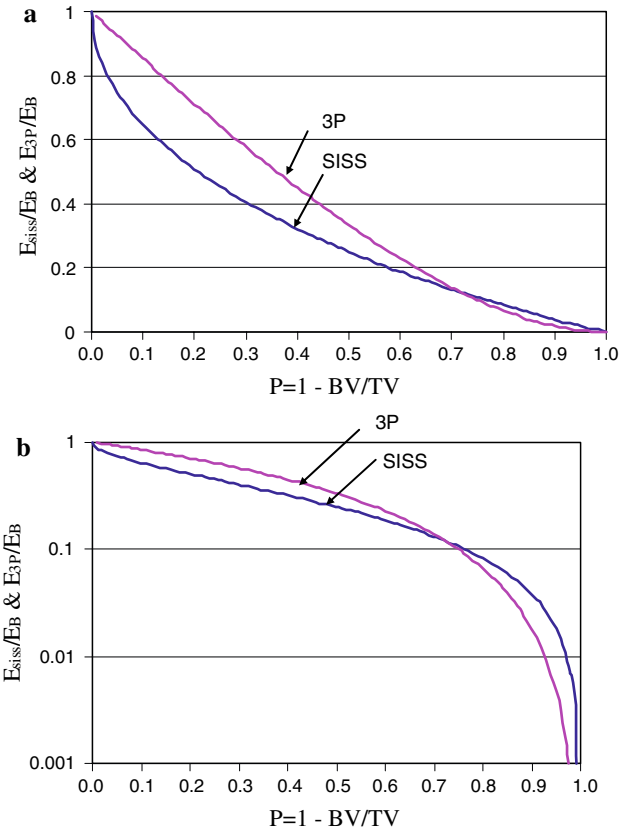

Fig. 2 Comparison between SISS model and 3P model for isotropic structure at the first level. **a** In a normal coordinate and **b** in a logarithmic coordinate

range of Young's modulus using the general variation range of another component parameter for common porous bones, such as mineral ratio from 0.4 to 0.85. The predictions shown in Fig. 5a and b are based on the maximum and minimum values of Young's modulus for the two levels of structure with the anisotropy of $\delta_z = 50\%$ and $\delta_x = \delta_y = 0$.

Figure 5a shows the predictions compared with the proximal/distal-measured data for compact bones where 115 data points were read out from Fig. 3 of [43] with the porosity from 20 to 80%, and 70 data points were from [45–47] with MR from 0.45 to 0.80 and porosity from 3 to 40%.

Figure 5b shows the predictions and the measured data for cancellous bones where the Young's modulus was measured in each of the 3 orthogonal directions of the cube samples and totally 165 data points were read out from Fig. 2 of [38] with the porosity from 40 to 96%. In addition, 20 data points of lateral/medial-measured Young's modulus with MR from 0.45 to 0.65 and porosity from 40 to 80% from [40–44] were displayed in Fig. 5b for comparison.

From Fig. 5a and b, one can see that, the measured data from multiple sources, except very few points, fall within the ranges of the predictions.

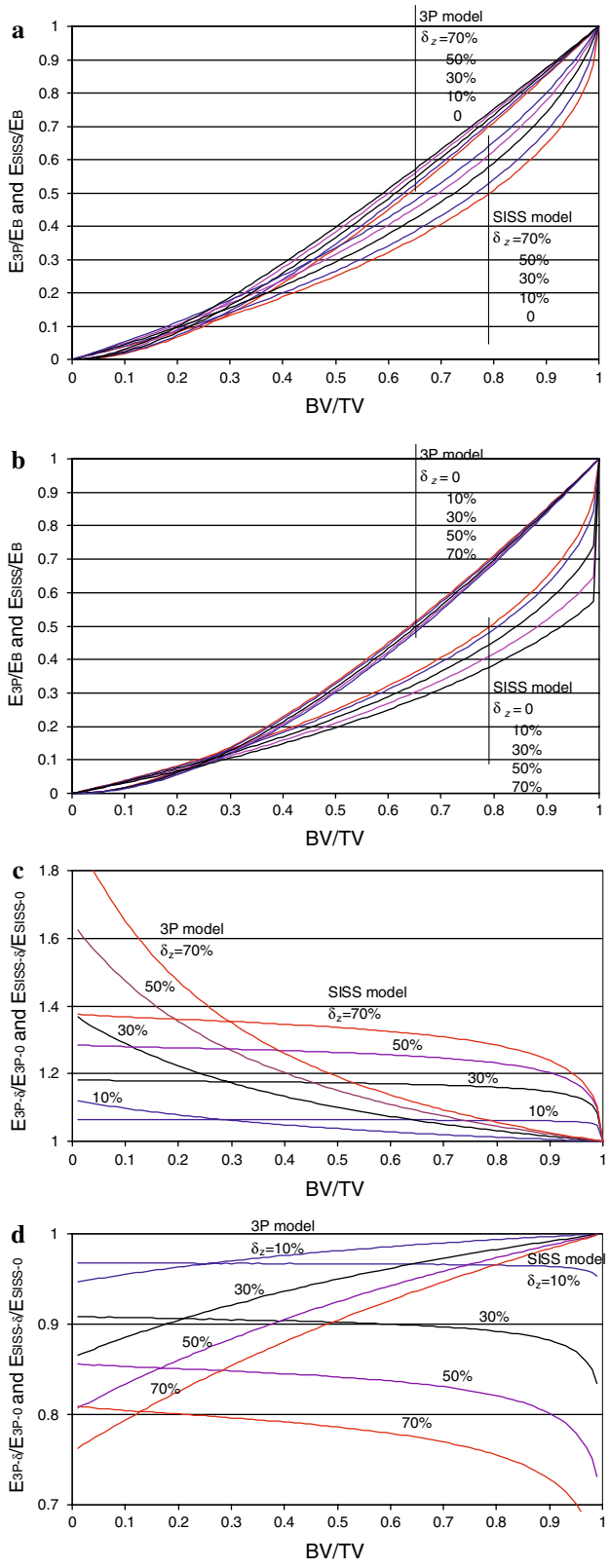

Fig. 3 Effect of anisotropy at z direction on SISS and 3P models with δ_z from 0 to 70% and $\delta_x = \delta_y = 0$. **a** Young's modulus at z direction, **b** Young's modulus at x or y direction, **c** ratio of Young's modulus at z direction, and **d** ratio of Young's modulus at x or y direction

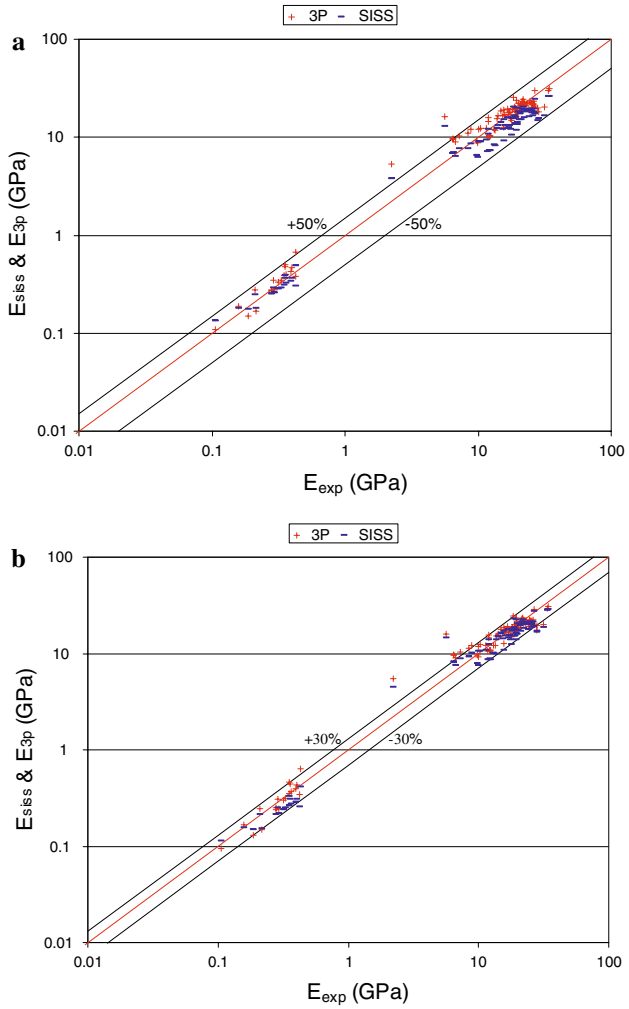

Fig. 4 Predictions of Young's modulus compared with 90 measured data of porous bones with *MR* ranging from 0.45 to 0.80 and porosity from 3 to 80% from [40–47]. **a** Predictions for the first level of isotropic structure ($\delta_x = \delta_y = \delta_z = 0$) and the second level of anisotropic structure. **b** Predictions for both levels of anisotropic structure ($\delta_z = 50\%$ and $\delta_x = \delta_y = 0$)

4 Discussion

4.1 Structural variations

Observations such as [13–20] have confirmed that, the overall morphology of porous bones is more "rod-like" at high porosities and more "plate-like" at relatively low porosities, and the "rod-like" solid bones often begin to become visible at a porosity higher than 70% ($BV/TV < 30\%$) for trabecular or cancellous bones. This can be explained by the findings of this work. The porous bones adapt their microstructures for maintaining higher stiffness by possessing a certain amount of solid bones. The critical porosity of the structural conversion from observations

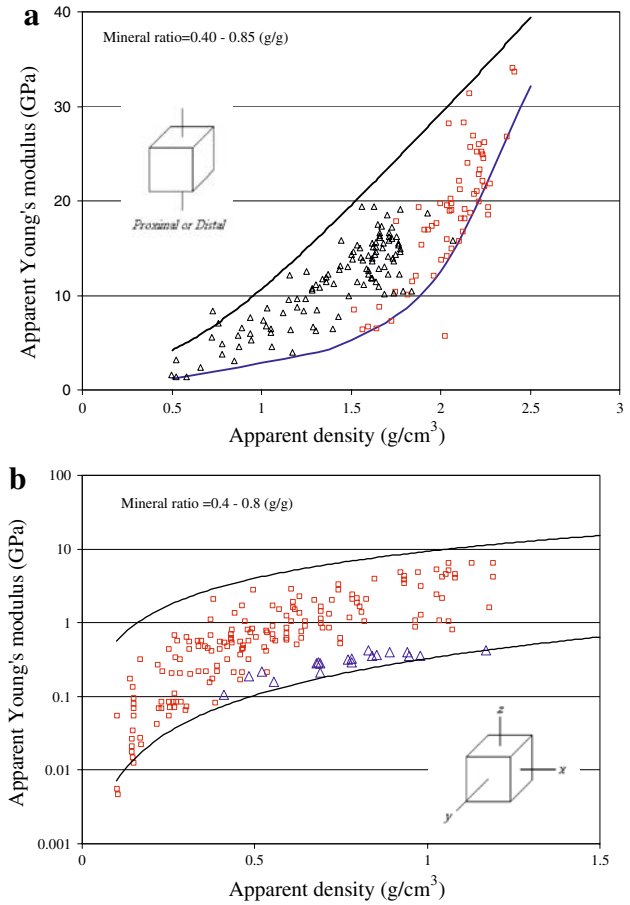

Fig. 5 Predictions of Young's modulus variation ranges for porous bones with anisotropy $\delta_z = 50\%$ and $\delta_x = \delta_y = 0$, compared with measured data with apparent density provided. **a** Predictions of maximum and minimum Young's modulus at the proximal/distal direction for compact bones with *MR* ranging from 0.40 to 0.85, compared with measured data from [44] with porosity of 20–80% (*triangles*) and measured data from [45–47] with *MR* of 0.45–0.8 and porosity of 3–40% (*squares*). **b** Predictions of maximum and minimum Young's modulus for cancellous bones with *MR* ranging from 0.40 to 0.80 compared with the data measured at each of 3 orthogonal directions of cube samples with porosity of 40–96% from [38] (*squares*) and the data measured at the lateral/medial direction with *MR* of 0.45–0.65 and porosity of 40–80% from [40–43] (*triangles*)

[13–20] is consistent with the model prediction, about 70%, as shown in Figs. 2a, b and 3a, b).

Moreover, the deterioration of cancellous bone structure due to aging or disease is characterised by a conversion from plate-like to rod-like accompanied with bone losses [19, 20]. The predictions by the proposed model show that, whether the stiffness increases or decreases with the solid bone shape change from "plate-like" to "rod-like" depends on the scale of porosity being greater or less than the critical porosity. In other words, the elasticity of a porous bones is determined by both its solid bone shape and porosity.

4.2 Model predictions

The power-law equation models, commonly elasticity–density relationships, usually have limited applicability, and the difference of predictions using the power-law models from different sources is as large as several folds to several ten folds [10, 39, 44]. Figure 4a shows a prediction accuracy of ±50% using the proposed model with the first level of isotropic structure and the second level of anisotropic structure. With the incorporation of anisotropy of $\delta_z = 50\%$ at the first level of structure into the modelling, as shown in Fig. 4b, the prediction accuracy is further increased to ±30%. Moreover, from Fig. 5a and b, it is known that the proposed model provides accurate predictions for the range of the modulus for cortical and cancellous bones.

Therefore, compared with the conventional power-law models, the proposed model has made marked progress. To the author's knowledge, this is the first time to use a single model to predict the stiffness with reasonable accuracy for all sorts of porous bones including cortical and cancellous.

4.3 Sources of prediction errors

Regarding the errors of measured data, a variety of sources—such as the test method, test condition, and the sample shape and state as mentioned by [48]—are likely. For modelling calculations at the first level of structure, the solid bone shape variations and anisotropy of the porous bones are the most recognisable sources; however, practically reliable techniques to quantify the solid bone shape variations and the anisotropy are still very few [2]. In this work, the solid bone shape of porous bones was supposed to vary between the two boundaries, the SISS and 3P model structures. A method to quantify the anisotropy at the first level of structure was proposed based on the three-dimensional average unit size difference. From Figs. 4b and 5a, b, the predictions using the proposed model for porous bones appear to be satisfactory. In addition, it may be promising to further improve the modelling accuracy by quantifying the fractions of plate-like and rod-like structures in a composite structure.

At the second level of structure, one of the likely sources of errors is that fixed values of geometric size, density, and modulus of the components of solid bones were chosen in advance for the modelling calculations. As were observed recently, Young's modulus and the geometric sizes of the components vary within a certain range [37]. Therefore, it is necessary to conduct further tests and observations in order to obtain average quantities with a higher degree of accuracy. Moreover, the mineral particles are essentially anisotropic so it is important to accurately evaluate the dimension numbers for the modelling calculations using

Eq. 18. In addition, the quantitative effect of water and lipid contents on the modulus of the organic phase is still not known [27, 34–36].

5 Conclusions

(1) A model with three compositional phases and two levels of hierarchical organization was proposed for predicting Young's modulus of porous bones. This model is based on the geometric similarity between porous bones and metal foams, and encompasses the microstructural variations and the anisotropy of two levels of organization.

(2) The SISS model and 3P model were shown to represent the two boundary models of "rod-like" and "plate-like" solid bones respectively. It has been demonstrated that the proposed model, including the SISS and 3P submodels combined with an anisotropic submodel for solid bones, provides predictions of Young's modulus with high accuracy up to ±30% for all sorts of porous bones over the entire range of porosities compared with measured data from the literature.

(3) The stiffness of porous bones depends on not only the solid bone shape ("rod-like", "plate-like" or combined) but also the porosity. Of the two submodels, the SISS model has a higher Young's modulus value than the 3P model when the porosity is greater than 70%, and a lower value when the porosity is less than 70%. This may explain why the structural conversion of trabecular bones from "plate-like" to "rod-like" often occurs at a porosity of about 70% or higher (*BV/TV* about 30% or lower) according to observations.

Acknowledgements Thanks to Professor John D. Currey for helpful suggestions and to Dr. Yun-Long Chang for constructive discussion about the microstructure of porous bones.

References

1. Fratzl P, Weinkamer R. Nature's hierarchical materials. Prog Mater Sci. 2007;52:1263–334.
2. Torquato S. Random heterogeneous materials. 1st ed. New York: Springer; 2002. Chapt. 1, 1–16; Chapt. 21–22, 552–631.
3. Maxwell JC. A treatise on electricity and magnetism. 3rd ed. New York: Dover Publications Inc.; reprinted 1954. Chapter 9.
4. Landauer R. The electrical resistance of binary metallic mixtures. J Appl Phys. 1952;23:779–84.
5. Wang JF, Carson JK, North MF, Cleland DJ. A new structural model of effective thermal conductivity for heterogeneous materials with co-continuous phases. Int J Heat Mass Transf. 2008; 51(9–10):2389–97.
6. Wang JF, Carson JK, North MF, Cleland DJ. A new approach to modelling the effective thermal conductivity of heterogeneous materials. Int J Heat Mass Transf. 2006;49(17–18):3075–83.
7. Wang JF, Carson JK, Willix J, North MF, Cleland DJ. A symmetric and interconnected skeleton structural (SISS) model for predicting thermal and electrical conductivity and Young's modulus of porous foams. Acta Mater. 2008;56(18):5138–46.
8. Currey JD. Bones-structure and mechanics. 1st ed. Princeton University Press; 2006.
9. Gibson LJ, Ashby MF. Cellular solids—structure and properties. 2nd ed. London: Cambridge; 1997.
10. Helgason B, Perilli E, Schileo E, Taddei F, Brynjolfsson S, Viceconti M. Mathematical relationships between bone density and mechanical properties: A literature review. Clin Biomech. 2008;23:135–46.
11. Sandino C, Planell JA, Lacroix D. A finite element study of mechanical stimuli in scaffolds for bone tissue engineering. J Biomech. 2008;41:1005–14.
12. Jones AC, Arns CH, Hutmacher DW, Milthorpe BK, Sheppard AP, Knackstedt MA. The correction of pore morphology, interconnectivity and physical properties of 3D ceramic scaffolds with bone ingrowth. Biomaterials. 2009;30:1440–51.
13. Hildebrand T, Laib A, Muller R, Dequeker J, Ruegsegger P. Direct three-dimensional morphometric analysis of human cancellous bone: microstructural data from spine, femur, iliac crest and calcaneus. J Bone Miner Res. 1999;14(7):1167–74.
14. Lazenby RA, Cooper DML, Angus S, Hallgrimsson B. Articular constraint, handedness, and directional asymmetry in the human second metacarpal. J Hum Evol. 2008;54:875–85.
15. van Ruijven LJ, Giesen EBW, Mulder L, Farella M, van Eijden TMGJ. The effect of bone loss on rod-like and plate-like trabeculae in the cancellous bone of the mandibular condyle. Bone. 2005;36:1078–85.
16. Ding M, Odgaard A, Danielsen CC, Hvid I. Mutual associations among microstructural, physical and mechanical properties of human cancellous bone. J Bone Joint Surg. 2002;84B(6):900–7.
17. Nicholson PHF, Muller R, Cheng XG, Puegsegger P, van der Perre G, Dequeker J, et al. Quantitative ultrasound and trabecular architecture in the human calcaneus. J Bone Miner Res. 2001; 16(10):1886–92.
18. Day JS, Sumner DR, Waarsing JH, Weinans H. Inter-individual and gender differences in bone adaptation strategy. In: Proceedings of 50th annual meeting of the Orthopaedic Research Society, Paper No. 0400; 2004.
19. Hildebrand T, Ruegsegger P. Quantification of bone microarchitecture with the structure model index. Comput Methods Biomech Biomed Eng. 1997;1(1):15–23.
20. van der Linden JC, Day JS, Verhaar JAN, Weinans H. Altered tissue properties induce changes in cancellous bone architecture in aging and diseases. J Biomech. 2004;37:367–74.
21. Seto J, Gupta HS, Zaslansky P, Wagner HD, Fratzl P. Tough lessons from bone: extreme mechanical anisotropy at the mesoscale. Adv Funct Mater. 2008;18(13):1905–11.
22. Sevostianov I, Kovacik J, Simancik F. Elastic and electric properties of closed-cell aluminium foams: cross-property connection. Mater Sci Eng A. 2006;420(1–2):87–99.
23. Goodall R, Weber L, Mortensen A. The electrical conductivity of microcellular metals. J Appl Phys. 2006;100:AN044912.
24. Hatta H, Taya M. Effective thermal conductivity of a misoriented short fibre composite. J Appl Phys. 1985;58(7):2478–86.
25. Jager I, Fratzl P. Mineralized collagen fibril: a mechanical model with a staggered arrangement of mineral particles. Biophys J. 2000;79:1739–46.
26. White ET, Tan WH, Ang JM, Tait S, Litster JD. The density of a protein crystal. Power Technol. 2007;179:55–8.
27. Hedges RW, Jacob AE. Phonons and the elastic moduli of collagen and muscle. Nature. 1977;267:285–7.
28. Snyders R, Music D, Sigumonrong D, Schelnberger B, Jensen J, Schneider JM. Experimental and ab initio study of the mechanical

properties of hydroxyapatite. Appl Phys Lett. 2007;90:193902-1,3.
29. Snyders R, Bousser E, Music D, Jensen J, Hocquet S, Schneider JM. Influence of the chemical composition on the phase constitution and the elastic properties of RF-sputtered hydroxyapatite coatings. Plasma Process Polym. 2008;5:168–74.
30. Viswanath B, Raghavan R, Ramamurty U, Ravishankar N. Mechanical properties and anisotropy in hydroxyapatite single crystals. Scripta Mater. 2007;57:361–4.
31. Sha MC, Li Z. Single-crystal elastic constants of fluorapatite, Ca5F(PO4)3. J Appl Phys. 1994;75(12):7784–7.
32. Katz JL, Ukraincik K. On the anisotropic elastic properties of hydroxyapatite. J Biomech. 1971;4:221–7.
33. Katz JL. Hard tissue as a composite material I. bounds on the elastic behaviour. J Biomech. 1971;4:455–73.
34. Grant CA, Brockwell DJ, Radford SE, Thomson NH. Effects of hydration on the mechanical response of individual collagen fibrils. Appl Phys Lett. 2008;92:233902-1,3.
35. Heim AJ, Mattews WG. Determination of the elastic modulus of native collagen fibrils via radial indentation. Appl Phys Lett. 2006;89:181902-1,3.
36. Wenger MPE, Bozec L, Horton MA, Mesquida P. Mechanical properties of collagen fibrils. Biophys J. 2007;93:1255–63.
37. Burger C, Zhou HW, Wang H, Sics I, Hsiao BS, Chu B, et al. Lateral packing of mineral crystals in bone collagen fibrils. Biophys J. 2008;95:1985–92.
38. Hodgskinson R, Currey JD. Young's modulus, density and material properties in cancellous bone over a large density range. J Mater Sci: Mater Med. 1992;3:377–81.
39. Morgan EF, Bayraktar HH, Keaveny TM. Trabecular bone modulus–density relationships depend on anatomic site. J Biomech. 2003;36:897–904.
40. Kang Q, An YH, Friedman RF. Mechanical properties and bone densities of canine trabecular bone. J Mater Sci: Mater Med. 1998;9:263–7.
41. Cavani F, Giavaresi G, Fini M, Bertoni L, Terlizzi FD, Barkmann R, et al. Influence of density, elasticity, and structure on ultrasound transmission through trabecular bone cylinders. IEEE Trans Ultrason Ferroelectr Freq Control. 2008;55(7):1465–71.
42. Fox J, Newman MK, Turner CH, Guldberg RE, Varela A, Smith SY. Effects of treatment with parathyroid hormone 1–84 on quantity and biomechanical properties of thoracic vertebral trabecular bone in ovariectomized rhesus monkeys. Calcif Tissue Int. 2008;82:212–20.
43. Hoffmeister BK, Johnson DP, Janeski JA, Keedy DA, Steinert BW, Viano AM, et al. Ultrasonic characterization of human cancellous bone in vitro using three different apparent backscatter parameters in the frequency range 0.6–150 MHz. IEEE Trans Ultrason Ferroelectr Freq Control. 2008;55(7):1442–52.
44. Keller TS, Mao Z, Spengler DM. Young's modulus, bending strength, and tissue physical properties of human compact bone. J Orthop Res. 1990;8(4):592–603.
45. Spatz HC, O'Leary EJ, Vincent TFV. Young's moduli and shear moduli in cortical bone. Proc R Soc Lond B: Biol Sci 1996;263(1368):287–94.
46. Schaffler MB, Burr DB. Stiffness of compact bone: effects of porosity and density. J Biomech. 1988;21(1):13–6.
47. Currey JD. The effect of porosity and mineral content on the Young's modulus of elasticity of compact bone. J Biomech. 1988;21(2):131–9.
48. Bevill G, Easley SK, Keaveny TM. Side-artifact errors in yield strength and elastic modulus for human trabecular bone and their dependence on bone volume fraction and anatomic site. J Biomech. 2007;40:3381–8.